SWITCHING CONTROL IN ACTIVE VIBRATION ISOLATION

M.F. Heertjes
Eindhoven University of Technology
Department of Mechanical Engineering
5600 MB Eindhoven, The Netherlands
m.f.heertjes@tue.nl

N. van de Wouw
Eindhoven University of Technology
Department of Mechanical Engineering
5600 MB Eindhoven, The Netherlands
n.v.d.wouw@tue.nl

W.P.M.H. Heemels
Eindhoven University of Technology
Department of Mechanical Engineering
5600 MB Eindhoven, The Netherlands
w.p.m.h.heemels@tue.nl

Abstract

In this paper, a switching control approach is studied with applications to active vibration isolation. The control design is based on the concept of input-to-state stability of the resulting discontinuous feedback system with respect to disturbances. The switching control strategy demonstrates improved disturbance rejection under feedback combined with a small sensitivity to noise in the absence of such feedback. Herein the control effort needed to achieve improved performance is substantially reduced. To access the performance of the closed-loop system, the control scheme is tested on a commercially available isolation system.

Key words

Absolute stability, discontinuous variable gains, switching systems, vibration isolation.

1 Introduction

In high-precision motion systems, vibration isolation is used to isolate (sub-)systems from environmental disturbances such as floor vibrations and acoustic excitations. Examples include electron microscopes for nano-scale imaging and wafer scanners for the manufacturing of integrated circuits. In these systems, vibration isolation performance is obtained both passively and actively. Herein active vibration isolation addresses both feed-forward and feedback control design. In terms of feedback control, the discrimination between high-frequent disturbances for which the isolated system is sensitive and low-frequent disturbances for which it is not (Hrovat, 1997) is key to isolation performance. The additional discrimination between small-amplitude steady-state responses and large-amplitude transients provides the means to improve this performance even further.

Envisioning such improvements starts with the observation that passive isolation typically relates to steady-state operation, *i.e.*, the kind of isolation for which the isolator is designed to achieve performance. Only in the incident of having large-amplitude transient responses (and corresponding disturbances) active control is actually needed to improve upon the error response. In fact, the injection of additional (measurement) noise resulting from closing the loop is largely unnecessary and undesirable in steady-state. It can be avoided by adopting the following switching control strategy: feedback control is switched on only when the system's response exceeds a pre-defined threshold value. Hence a further increase of the transient response is avoided but at the cost of an increased (measurement) noise sensitivity. Below the threshold value, the control is switched off. This keeps the steady-state response limited in amplitude whereas the high-frequency isolation properties corresponding to the passive isolator design remain valid. Moreover, the control effort is kept small and so is the injection of noise by closing the loop. A comparable strategy is known to improve upon the disturbance rejection properties of optical storage drives, see (Baek, *et al.*, 2006; Van de Wouw, *et al.*, 2007). The approach in this paper is different because of the discontinuous nature of the switching (Liberzon, 2003), which requires a careful analysis of the resulting closed-loop system as it is known that favorable properties (*e.g.*, stability) are not always maintained in discontinuous closed-loop systems. In the problem of vibration isolation considered here, we will prove that the desirable properties of the subsystems based on passive isolation and active control remain in the switched system. We will use the concepts of input-to-state stability (Sontag, 1995) and extensions of absolute stability theory (Yakubovich, *et al.*, 2004; Materassi, *et al.*, 2007) to show this.

The paper is further organized as follows. In Section 2, a representative vibration isolation system is discussed. In Section 3, the switching control strategy is introduced as a means to improve upon isolator performance by active damping. In Section 4, stability properties induced by this strategy are studied. In Section 5, experimental results are discussed, and in Section 6,

a brief overview of the key observations is presented.

2 Vibration Isolation

Vibration isolation is used, for example, in the wafer scanner industry where a so-called metrology frame is isolated from environmental disturbances. This metrology frame contains interferometers consisting of lasers, mirrors, and other measuring devices, and provides a position reference for nano-scale position control of the wafer scanner's main motion control systems, see (Van de Wal, *et al.*, 2002) for a brief system description.

An example of such a metrology frame, which is used as an experimental benchmark in this study, is depicted in Figure 1. It shows a payload mass of 1000 kg

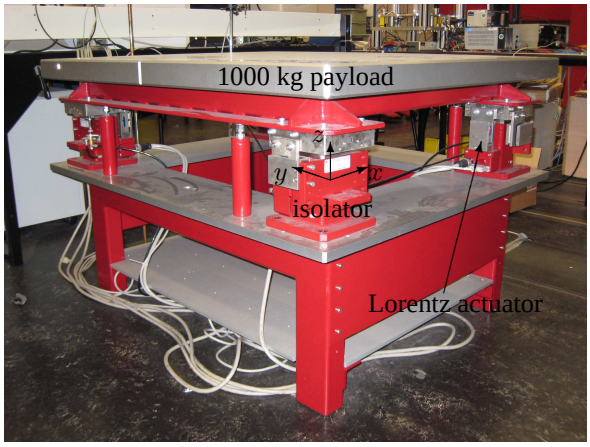

Figure 1. Vibration isolation system.

which is supported by four pneumatic isolators. The natural frequency of the passive system in the vertical z-direction is 3.24 Hz. Because the passive system is weakly damped, six Lorentz actuators and six geophones – the latter for velocity measurement – provide the means to actively damp the system; three of each in both the horizontal and the vertical direction. In the absence of such active damping, the behavior of the isolation system is shown in Figure 2, which involves a typical measurement series. Through time-frequency analysis, the figure shows the scaled magnitude of the z-velocity response of the payload both in time- and frequency-domain. The magnitude is linearly scaled from deep red (small) to deep blue (large). In the response, large non-stationary oscillations near 3.24 Hz are clearly recognized.

3 Active Damping by Switching Control

To improve the payload response, we reside to active damping by switching control. Herein the simplified control representation of Figure 3 is used where the passive isolation system, represented by the transfer function $\mathcal{H}(s)$, is controlled using a control force f_c.

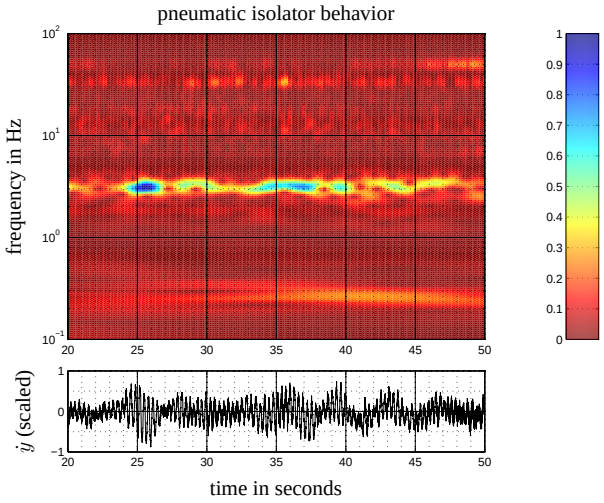

Figure 2. Time-frequency analysis of the measured z-velocity without active damping.

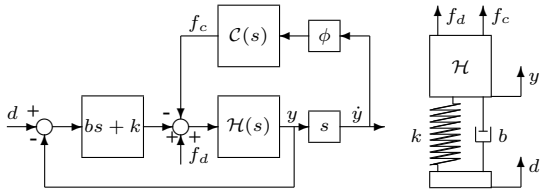

Figure 3. Simplified schematic of a controlled vibration isolator along with a mechanical representation.

A fourth-order isolator model is given by

$$\mathcal{H}(s) = \frac{m_2 s^2 + b_{12} s + k_{12}}{m_1 m_2 s^4 + (m_1 + m_2)(b_{12} s^3 + k_{12} s^2)}, \tag{1}$$

with $m_1 = 950$ kg, $m_2 = 50$ kg, $b_{12} = 3 \cdot 10^2$ Nsm^{-1}, and $k_{12} = 1.75 \cdot 10^6$ Nm^{-1}. The isolation system is subjected to environmental disturbances d (floor vibrations) and f_d (acoustic excitations) and a controller force f_c. Given the payload velocity $\dot{y}$, the controller transfer function $\mathcal{C}(s)$ from $\dot{y}$ to f_c is given by

$$\mathcal{C}(s) = k_d \left\{ \frac{s}{s + \omega_{hp}} \right\}^2 \left\{ \frac{\omega_{lp}}{s + \omega_{lp}} \right\}^2, \tag{2}$$

with k_d a gain, ω_{hp} the cross-over frequency of a second-order high-pass filter, and ω_{lp} the roll-off frequency of a second-order low-pass filter. $\mathcal{C}(s)$ reflects a complex-valued damper and is used to improve disturbance rejection near resonance without significantly deteriorating the passive isolation properties which are characterized by the isolator stiffness k and its damping coefficient b in combination with $\mathcal{H}(s)$. The choices for ω_{hp} and ω_{lp} are related to sensor and actuator limitations. For the given geophone velocity measurement,

sensor limitations typically occur below 0.1 Hz which lead to the choice for $\omega_{hp} = 0.2\pi$ rad/s. Actuator limitations occur beyond 100 Hz, hence $\omega_{lp} = 200\pi$ rad/s.

For the system depicted in Figure 1, the characteristics given by the transfer function from f_d to $\dot{y}$:

$$\mathcal{O}_l(s) = \frac{s\mathcal{H}(s)}{1 + (bs + k)\mathcal{H}(s) + s\phi\mathcal{C}(s)\mathcal{H}(s)}, \qquad (3)$$

are depicted in Figure 4 (for $s = 2\pi j f$ and frequency

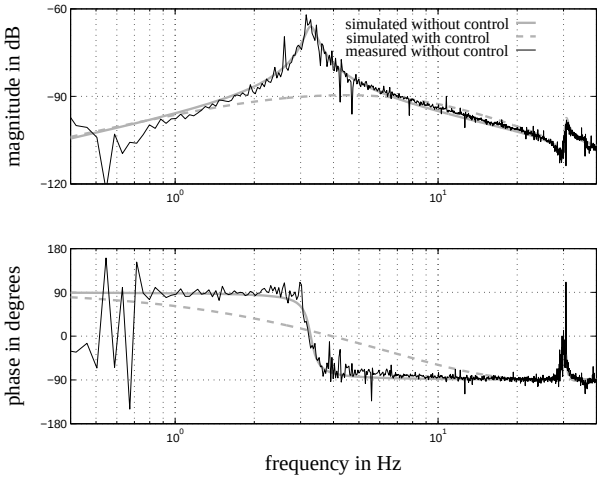

Figure 4. Bode representation of the isolator characteristics $\mathcal{O}_l$ with ($\phi = 1$) or without ($\phi = 0$) control.

f) either with ($\phi = 1$) or without ($\phi = 0$) control. In Bode representation, the results reflect both measurements and simulations. From the figure, it is clear that isolator performance benefits from the given control: the natural frequency is heavily suppressed whereas high-frequent isolator properties largely remain valid.

The validity of this observation is shown in Figure 5 using time-frequency analysis. In comparison with Figure 2, it can be seen that the velocity response is indeed significantly reduced in amplitude. The non-stationary oscillations dominated by the natural frequency of the passive isolator seem no longer present. However, the price paid is an amplification of high-frequent noise (between 10-20 Hz). This is seen more clearly in Figure 6 by subjecting the corresponding scaled control force to a similar analysis. In achieving performance, the linear controller induces a significant high-frequent output which is undesirable as this kind of controller output should be avoided in preserving high-frequent passive isolation. Moreover, the controller output shows activity in the low-frequency range where the geophone velocity measurement becomes invalid. These observations hint toward the application of a switching control. Sporadically switching the control on improves the resonance-induced isolator response related to large-amplitude transients. Switching the

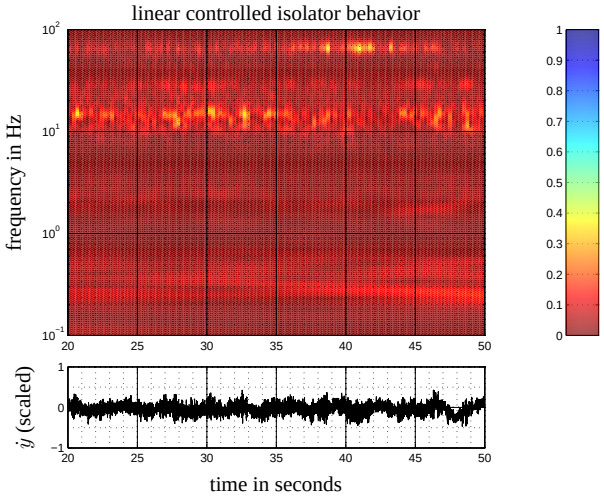

Figure 5. Time-frequency analysis of the measured and linear controlled z-velocity.

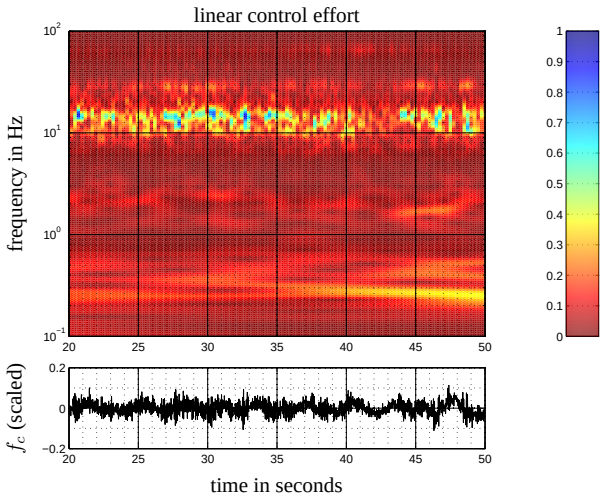

Figure 6. Time-frequency analysis of the measured control force in z-direction.

control off restores the passive isolation properties, at least intuitively, which are favorable in view of low-amplitude steady-state noise.

Key to the switching gain control design in Figure 3 is the choice of selector (or switch) function $\phi(\cdot)$, or

$$\phi(\dot{y}) = \begin{cases} 0, \text{ if } |\dot{y}| \leq \delta \\ 1, \text{ if } |\dot{y}| > \delta, \end{cases} \qquad (4)$$

where $\delta \geq 0$. This selector function discriminates between control ($\phi(\cdot) = 1$) and no control ($\phi(\cdot) = 0$) on the basis of the magnitude of the input signal $\dot{y}(t)$. Its characteristics are depicted in Figure 7. The analysis of the switching control system behavior is nontrivial (Liberzon, 2003; Armstrong, *et al.*, 2006) and one should be cautious not to jump in any conclusions. In fact, we need a thorough study of its stability and performance properties.

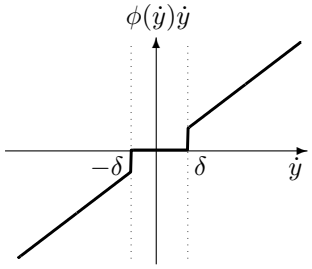

Figure 7. Switching characteristics of $\phi(\dot{y})\dot{y}$.

4 Stability for the Switching Control Strategy

Stability of the closed-loop system for the switching control strategy directly relates to the distinction between transient and steady-state disturbances. Transient disturbances are assumed to occur incidentally. When present, they often cause the system to react heavily in terms of error response. Control then mainly improves upon this response. In case these transient disturbances are absent, the error response caused by steady-state noise is typically small enough to validate the absence of control, *i.e.*, $|\dot{y}(t)| \leq \delta$. This restores then the passive isolation properties. From stability point of view it is therefore sufficient to require that the control – if applied – forces the system response toward the uncontrolled (passive) steady-state. We will use the concept of input-to-state stability (Sontag, 1995) to show that, first, the closed-loop system will exhibit bounded responses to any bounded disturbance both transient and steady-state and, second, passive isolation behavior will be retained in the absence of these transient disturbances.

Input-to-state stability is studied using the following system representation

$$\begin{aligned} \dot{x}_1 &= Ax_1 + bu_1 + bv \\ y_1 &= c^{\mathrm{T}}x_1 = \dot{y} \\ u_1 &= -\phi(y_1)y_1, \end{aligned} \tag{5}$$

with state vector $x_1(t)$, control input $u_1(t)$, disturbance $v(t)$ and output $y_1(t)$. The relation between the disturbance input $v(t)$ and the disturbances $d(t)$ and $f_d(t)$ in Figure 3 is given by

$$\mathcal{L}\{v(t)\} = -\mathcal{C}^{-1}(s)\left(\mathcal{L}\{f_d(t)\} + (bs+k)\mathcal{L}\{d(t)\}\right), \tag{6}$$

with $\mathcal{L}\{\cdot\}$ the Laplace operator on the corresponding signals. Furthermore, the matrices A, b, c follow from standard state-space realization arguments using the transfer functions related to Figure 3. Without making an explicit distinction between the transient and the steady-state parts contained in $v(t)$, we consider the Lyapunov function candidate $V(x_1) = x_1^{\mathrm{T}}Px_1$ for a positive definite matrix $P = P^{\mathrm{T}} > 0$. Note that

$$c_1\|x_1\|^2 \leq V(x_1) \leq c_2\|x_1\|^2, \tag{7}$$

with $c_1 = \lambda_{\min}(P)$ and $c_2 = \lambda_{\max}(P)$. Using the following positive real condition

$$\begin{aligned} A^{\mathrm{T}}P + PA &= -qq^{\mathrm{T}} - \epsilon P \\ Pb &= c - \sqrt{2}q, \end{aligned} \tag{8}$$

with $\epsilon > 0$, it follows that

$$\begin{aligned} \dot{V}(x_1) &= x_1^{\mathrm{T}}(A^{\mathrm{T}}P + PA)x_1 + 2x_1^{\mathrm{T}}Pbu_1 + 2x_1^{\mathrm{T}}Pbv \\ &\leq -\epsilon x_1^{\mathrm{T}}Px_1 - (x_1^{\mathrm{T}}q + \sqrt{2}u_1)^2 + 2x_1^{\mathrm{T}}Pbv \\ &\leq -\epsilon V(x_1) + 2x_1^{\mathrm{T}}Pbv, \end{aligned} \tag{9}$$

where we used the fact that $y_1u_1 \leq -u_1^2$ which follows from the characteristics depicted in Figure 7. The existence of a positive definite P in (8) implies that

$$\begin{aligned} &\Re\left\{c^{\mathrm{T}}(j\omega I - A)^{-1}b\right\} = \\ &\Re\left\{\frac{j\omega\mathcal{C}(j\omega)\mathcal{H}(j\omega)}{1 + (bj\omega + k)\mathcal{H}(j\omega)}\right\} \geq -1, \end{aligned} \tag{10}$$

which is the circle criterion interpretation (Yakubovich, *et al.*, 2004). With

$$2\|bv\|\|x_1\| \leq \alpha\|bv\|^2 + (1/\alpha)\|x_1\|^2, \tag{11}$$

for any $\alpha > 0$, (9) yields

$$\begin{aligned} \dot{V}(x_1) &\leq -\epsilon V(x_1) + c_2\left(\alpha\|bv\|^2 + \frac{1}{\alpha}\|x_1\|^2\right) \\ &\leq -\epsilon\beta V(x_1), \end{aligned} \tag{12}$$

when

$$\|x_1\| \geq \sqrt{\frac{c_2\alpha^2}{(1-\beta)\epsilon c_1\alpha - c_2}}\|b\|\|v\|_\infty, \tag{13}$$

with $0 < \beta < 1$ and $\|v\|_\infty = \sup_{t\geq 0}|v(t)|$. Equations (12) and (13) represent a Lyapunov characterization of the ISS of (5) from which it follows that

$$\|x_1(t)\| \leq \rho_\beta(\|x_1(0)\|, t) + \gamma_\beta(\|v\|_\infty), \tag{14}$$

with ρ_β a so-called $\mathcal{KL}$-function and γ_β a $\mathcal{K}$-function given by

$$\begin{aligned} \rho_\beta(\|x_1(0)\|, t) &= \sqrt{\frac{c_2}{c_1}}\|x_1(0)\|e^{-\frac{\epsilon\beta}{2}t} \\ \gamma_\beta(\|v\|_\infty) &= \sqrt{\frac{{c_2}^2\alpha^2}{(1-\beta)\epsilon {c_1}^2\alpha - c_1c_2}}\|b\|\|v\|_\infty, \end{aligned} \tag{15}$$

which guarantees a bounded state response for any bounded disturbance $v(t)$.

Additionally, (14) can be used to compute how large the ultimate bound is with respect to steady-state disturbances. At this point in the analysis we introduce the discrimination between transient and steady-state disturbances. If we assume $v(t)$ to consist only of steady-state disturbances then it follows from (14) that all solutions $x_1(t)$ are ultimately confined to a ball of radius $\gamma_\beta(\|v\|_\infty)$, hence

$$\limsup_{t\to\infty} \|x_1(t)\| \leq \gamma_0(\|v\|_\infty). \qquad (16)$$

Indeed, this shows, that if $\delta > \gamma_0(\|v\|_\infty)$, then the response induced by small steady-state disturbances is determined by the passive isolation dynamics only.

5 Performance for the Switching Control Strategy

Performance of the closed-loop system for the switching control strategy will be assessed (both in time- and frequency-domain) at the vibration isolation system depicted in Figure 4. This includes a comparison between no control, switching control, and linear control.

Through experimental evaluation, the result of the switching control in terms of measured isolator response is shown in Figure 8; herein the choice for $\delta = 0.2$ is based on trial-and-error by seeking the non-resonant signal levels of the passive system (see Figure 2) on the one hand and trying to minimize the control activity on the other hand. Similar to the linearly controlled isolator characteristics of Figure 5, the non-stationary oscillations related to the system's natural frequency have almost disappeared. But the amplification of high-frequent noises is no longer present. Hence the high-frequent passive isolation properties are preserved. This is shown more clearly when applying the time-frequency analysis to the switching (and scaled) control forces, the result of which is shown in Figure 9. As compared to the linear control forces depicted in Figure 6, it can be seen that control is only applied in those time intervals where the error response exceeds the threshold value δ. For the remaining intervals, no control is applied. The advantages are twofold: the high-frequent isolation deterioration such as encountered under linear control is avoided, and much less control effort is induced to achieve performance.

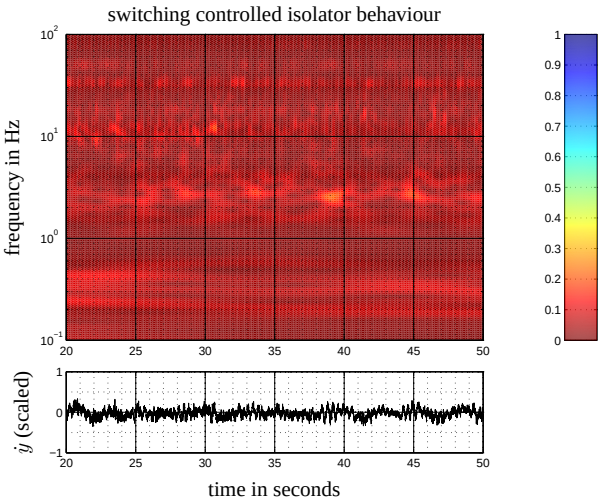

Figure 8. Time-frequency analysis of the measured and switching controlled z-velocity.

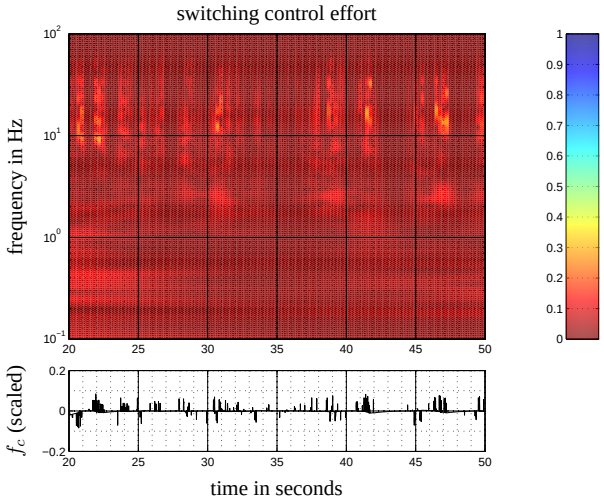

Figure 9. Time-frequency analysis of the measured switching control force.

In time-domain, Figure 10 more clearly illustrates the differences between the considered control strategies. For the scaled payload velocity in z-direction, it can

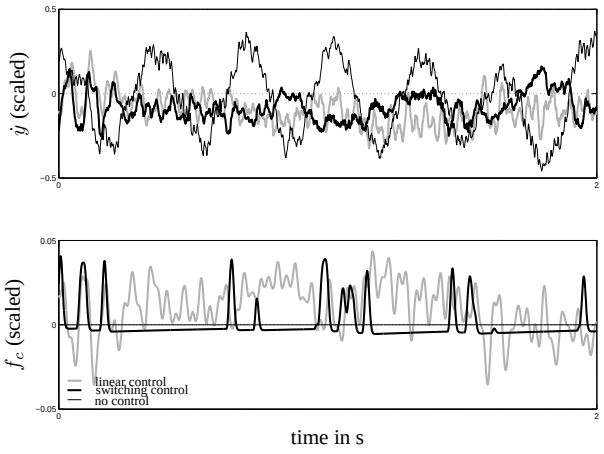

Figure 10. Time-series measurement of the payload velocity and control force in z-direction in case of no control, linear control, and switching control.

be seen that no control yields the expression of large oscillations (thin black curves) dictated by the weakly damped pneumatic system's resonance. Under linear control these oscillations disappear (grey curves) but the velocity response shows increased high-frequent oscillatory behavior. Switching control provides an effective means in dealing with the pneumatic system's resonance (thick black curves) but also limits the presence of high-frequent noise. This is mainly due to the fact that control is only sporadically switched on, which is shown in the lower part of the figure.

Similar observations are obtained from cumulative power spectral density (cpsd) analysis as can be found

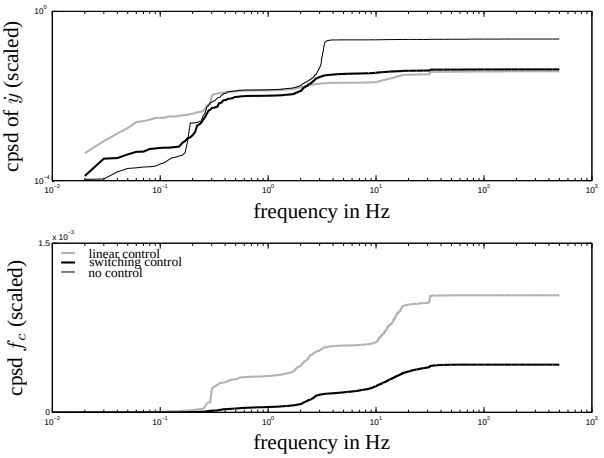

Figure 11. Cumulative power spectral density (cpsd) analysis of the payload velocity and control force in z-direction in case of no control, linear control, and switching control.

in Figure 11. From this figure it can be concluded that both linear and switching control give a similar root-mean-square (rms) value of the scaled velocity signals in z-direction. Each experiment corresponds to a time interval of 100 seconds in which a sampling frequency of 1 kHz is used. For switching control, the result is obtained with significantly less control effort, thus giving limited transmission (and amplification) of noise through control.

The relation between rms-performance and control effort is shown more clearly in Figure 12. By considering

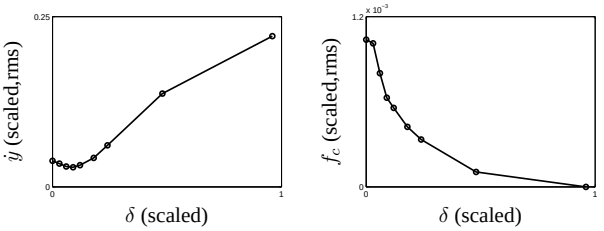

Figure 12. Root-mean-square (rms) values of the payload velocity and control force in z-direction under variation of δ.

several values for the threshold level δ, conducting nine cumulative power spectral density experiments such as considered in Figure 11, and depicting the resulting rms-values of each experiment as a function of δ, it can be seen that for sufficiently small δ the switching control competes with the linear control ($\delta = 0$) in terms of small rms-values but induces less control effort.

6 Conclusions

A switching control design is demonstrated to be effective in achieving improved active vibration isolation. Sporadically switching the control on effectively removes oscillations from the velocity response related to the weakly damped isolation system's resonance. The introduction of noise, typically occurring by closing the loop, is largely avoided by switching the control off for small velocities. Consequently, the control effort is kept small while preserving the desired passive isolation stability and performance properties.

References

Armstrong BSR, Gutierrez JA, Wade BA, and Joseph R. (2006) Stability of phase-based gain modulation with designer-chosen switch functions. International Journal of Robotics Research, 25:781-796.

Baek, J-S, Chung, CC, Tomizuka, M. (2006) Anti-shock controller design for optical disk drive systems with a nonlinear controller. *In Proceedings of the 2006 American Control Conference*, Minneapolis, MI, USA, pp. 1982–1989.

Heertjes MF, Cremers FLM, Rieck M, and Steinbuch M. (2005) Nonlinear control of optical storage drives with improved shock performance. Control Engineering Practice, 13:1295-1305.

Hrovat D. (1997) Survey of advanced suspension developments and related optimal control applications. Automatica, 33(10), pp. 1781–1817.

Liberzon, D. (2003) Switching in systems and control. Birkhäuser, Boston.

Materassi, D, Innocenti, G, Genesio, R and Basso, M. (2007) A composite circle criterion. *In Proceedings of the 46th Conference on Decision and Control*, New Orleans, LA, USA.

Sontag, ED. (1995) On the input-to-state stability property. European Journal of Control,1, pp. 24-36.

Wouw, van de N, Pastink, HA, Heertjes, MF, Pavlov, AV, and Nijmeijer, H. (2007) Performance of convergence-based variable-gain control of optical storage drives. Automatica, doi: 10.1017/ j.automatica.2007.04.004.

Wal, van de M, Baars, van G, Sperling F, and Bosgra O. (2002) Multivariable $\mathcal{H}_\infty/\mu$ feedback control design for high-precision wafer stage motion. Control Engineering Practice, 10, pp. 739-755.

Yakubovich, VA, Leonov, GA, and Gelig AKh. (2004) Stability of stationary sets in control systems with discontinuous nonlinearities. World Scientific, Singapore.